THE IGNITION AND COMBUSTION OF A LIQUID MONOPROPELLANT

By B. L. Karhan

Technical Memorandum
File No. TM 705.9161-01
May 18, 1967
Contract NOw 65-0123-d
Copy No. 22

The Pennsylvania State University
Institute for Science and Engineering
ORDNANCE RESEARCH LABORATORY
University Park, Pennsylvania

NAVY DEPARTMENT · NAVAL ORDNANCE SYSTEMS COMMAND

References: See page 64

Abstract: An investigation was made of the heat-up, ignition and combustion of a nitrate ester monopropellant droplet when suddenly placed in a high temperature gas. At moderate pressures a combustion zone became noticeably developed as the droplet approached its wet bulb temperature and a steady burning period followed. At high pressures reactive effects became noticeable early in the heat-up period and burning was not steady. In this regime the droplet spent most of its lifetime in the preignition period. A heat-up theory of ignition is developed and found to be in agreement with the moderate pressure data. Burning rates also reported over the test range.

ACKNOWLEDGMENTS

The author wishes to thank Professor Gerard M. Faeth, who supervised the research, for his encouragement and invaluable guidance throughout the course of the investigation. Thanks go, as well, to George Yanyecic for his assistance in the experimentation.

The author also wishes to express his sincere appreciation to the Ordnance Research Laboratory for its total financial support of the investigation.

TABLE OF CONTENTS

LIST OF FIGURES

NOMENCLATURE

A - Surface Area of Droplet (FT^2)

B - Radiation Absorption Coefficient (Dimensionless)

Bi - Dimensionless Biot Number

C - Burning Rate Constant (FT^2/SEC)

$C_{3,4}$ - Integration Constants

C_p - Specific Heat of Droplet ($BTU/LBM\,^oR$)

D - Droplet Diameter (FT)

D_o - Initial Droplet Diameter (FT)

$\bar{D}$ - Average Droplet Diameter During Burning Period (FT)

E - Activation Energy (BTU/MOL)

Gr - Dimensionless Grashof Number

H - Heat of Combustion (BTU/LBM)

h - Heat Transfer Coefficient ($BTU/FT^2\ SEC\,^oR$)

K - Rate Constant in Arrhenius Eq.

k - Liquid Thermal Conductivity ($BTU/FT\ SEC\,^oR$)

k_g - Gas Thermal Conductivity ($BTU/FT\ SEC\,^oR$)

L - Heat of Vaporization (BTU/LBM)

l_1 - Minor Axis of an Ellipsoid (FT)

l_2 - Major Axis of an Ellipsoid (FT)

$\dot{m}$ - Mass Burning Rate (LBM/SEC)

Nu - Dimensionless Nusselt Number

N - Order of Reaction (Dimensionless)

P - Pressure (LBF/FT^2)

P_R - Dimensionless Prandtl Number

Q - Radiation Absorbed Per Unit Volume (BTU/FT^3)

q - $H/C_p T_\infty$ = dimensionless

r - Radial Distance (FT)

r_E - Outer Radius of Droplet (FT)

r_o - Initial Droplet Radius (FT)

R_o - Universal Gas Constant ($BTU/MOL\,^oR$)

S - Transform Variable from Laplace Transformation

T - Droplet Temperature (^oR)

T_c - Flame Temperature (^oR)

T_E - Temperature of Droplet Surface (^oR)

T_o - Initial Droplet Temperature (^oR)

T_∞ - Furnace Temperature (^oR)

t_o - Fuel Time Constant (SEC)

t - Time (SEC)

V - Volume of Droplet (FT^3)

v_c - Velocity of Flame Surface (FT/SEC)

X - Frequency Factor in Arrhenius Expression

Y_n - Root of Trancendental Eq. TAN $Y_n = -Y_n$ / (Bi/2-1)

$Z_u = \sqrt{S}$

α = Constant = Bi/2, Dimensionless

β = Constant = α - 1 = Bi/2 - 1, Dimensionless

λ = $L/C_p T_\infty$ = Dimensionless

σ = Stefan-Boltzman Coefficient

σ_c = Dimensionless Ratio of Flame Radius to Drop Radius

ρ = Density of Droplet (LBM/FT^3)

ρ_c = Density of Gas at Flame Surface (LBM/FT^2)

θ = Dimensionless Temperature Difference

$\bar{\theta}$ = Dimensionless Temperature Difference in Transformed S-Domain

η = Dimensionless Radius

τ = Dimensionless Time

Ψ = Radiation Factor, Dimensionless

CHAPTER 1

INTRODUCTION

1.1 General Statement of the Problem

In recent years monopropellant droplet combustion has received an increasing amount of attention. While liquid monopropellants have not been found to be promising for use in the primary propulsion units of aircraft or missiles, they may be adapted to secondary applications. A thorough understanding of the combustion processes of a single monopropellant droplet is an important first step in comprehending the combustion process of these fuels in rocket motors. This thesis is concerned with an experimental and analytical investigation of the heat-up and burning rates of a particular liquid monopropellant when suddenly subjected to a high temperature environment.

1.2 Previous Related Studies

Regarding droplet combustion studies in general, Kobayasi[12] and Nishiwaki[17] introduced the use of an electrically heated movable furnace in their studies of bipropellant ignition. The heated furnace was moved over a droplet supported on a quartz fiber to provide rapid introduction of the droplet into the high

temperature environment. Motion pictures were taken of the heat-up and ignition of the droplet.

A technique similar to that of Kobayasi[12] and Nishiwaki[17] was applied to monopropellant combustion by Barrere[3] for a variety of monopropellants. Barrere[3] tested in a nitrogen environment at atmosphere pressure with ambient temperatures between 1000°F and 1600°F. Droplets with diameters between .030 and .080 inches were tested. However, primary emphasis was on the quasi-steady state burning period of the droplet and no ignition measurements were made.

Barrere's[3] test is the only study to date in which the monopropellant was apparently allowed to burn in an inert atmosphere as is the case in an engine where the monopropellant burns in its products of combustion. Tarifa, et al,[26] and Rosser[20] were able to support combustion only with the addition of oxygen to the environment thereby creating a system not truly represented as monopropellant combustion.

An early attempt at theoretically modeling the combustion of a motionless monopropellant droplet was undertaken by Borell and Wise[14]. Their model considered a chemical reaction diffused throughout the gas phase with the fuel vapor decomposing exothermically into product gases at a rate dependent on the temperature and weight fraction of the fuel vapor. By taking equal values of molecular weights and by assuming a Lewis number of unity, the

problem was solved by integrating numerically the resulting differential equations of the process.

Later works of Tarifa, et al[26], and Williams[28] considered diffusion of species of different molecular weights and Lewis numbers. Williams[28] presents exact results for his model by applying the assumption of a thin flame zone for reactions with sufficiently large activation energies. This model, first attributed to Spalding[24], allows direct simultaneous solution of the system equations. However, the general lack of experimental results has prevented any verification or revision of existing theories.

1.3 Specific Statement of the Problem

The preceding discussion has indicated that knowledge of the combustion processes of liquid monopropellants is, at best, very limited.

Concerning the existing theories of monopropellant droplet burning, it would be of interest to determine what limitations, if any, they present. Without this knowledge, the accuracy of burning lifetimes predicted by these theories is subject to question.

Also, it is of importance to understand the heat-up mechanism of a monopropellant. Its relationship to the heat-up time and, ultimately, to the total droplet lifetime must be a primary consideration in rocket engine design.

The technique employed by Barrere[3] offers a means of studying the droplet combustion process. However, by enclosing the apparatus in a pressure vessel equipped with a means of evacuation, a pure inert atmosphere may be maintained at various total pressures.

To summarize, the specific objectives of this thesis are as follows:

1. To formulate a theory for the heat-up and ignition of a motionless monopropellant droplet, and check it experimentally over a range of ambient temperatures and pressures.

2. To apply a suitable existing monopropellant burning theory to the experimental results, and thereby determine its limitations.

CHAPTER 2

EXPERIMENTAL APPARATUS AND PROCEDURE

2.1 Test Facility

The primary requirement of the experimental apparatus was to provide a means of rapidly placing a droplet into a high temperature inert atmosphere at various total gas pressures. A means of photographically recording the droplet's behavior and a means of measuring the droplet's temperature were also required.

A photograph of the experimental apparatus used for this study of the ignition and combustion of monopropellant droplets is shown in Figure 2.1. Figure 2.2 is a schematic diagram of the internal chamber assembly.

The upper part of the apparatus was enclosed with a pressure vessel which allowed operation up to 3,000 PSI. A hand-operated winch was used to raise and lower the upper cover and, when the cover was bolted to the base, the chamber was gas tight. By using a vacuum pump and a removable hose attached to a pressure sealed connector, the chamber was evacuated and then pressurized with the inert gas. For operating pressures below one atmosphere, the pressure within the chamber was measured with a differential mercury manometer. Measurement of chamber pressures between 1 and

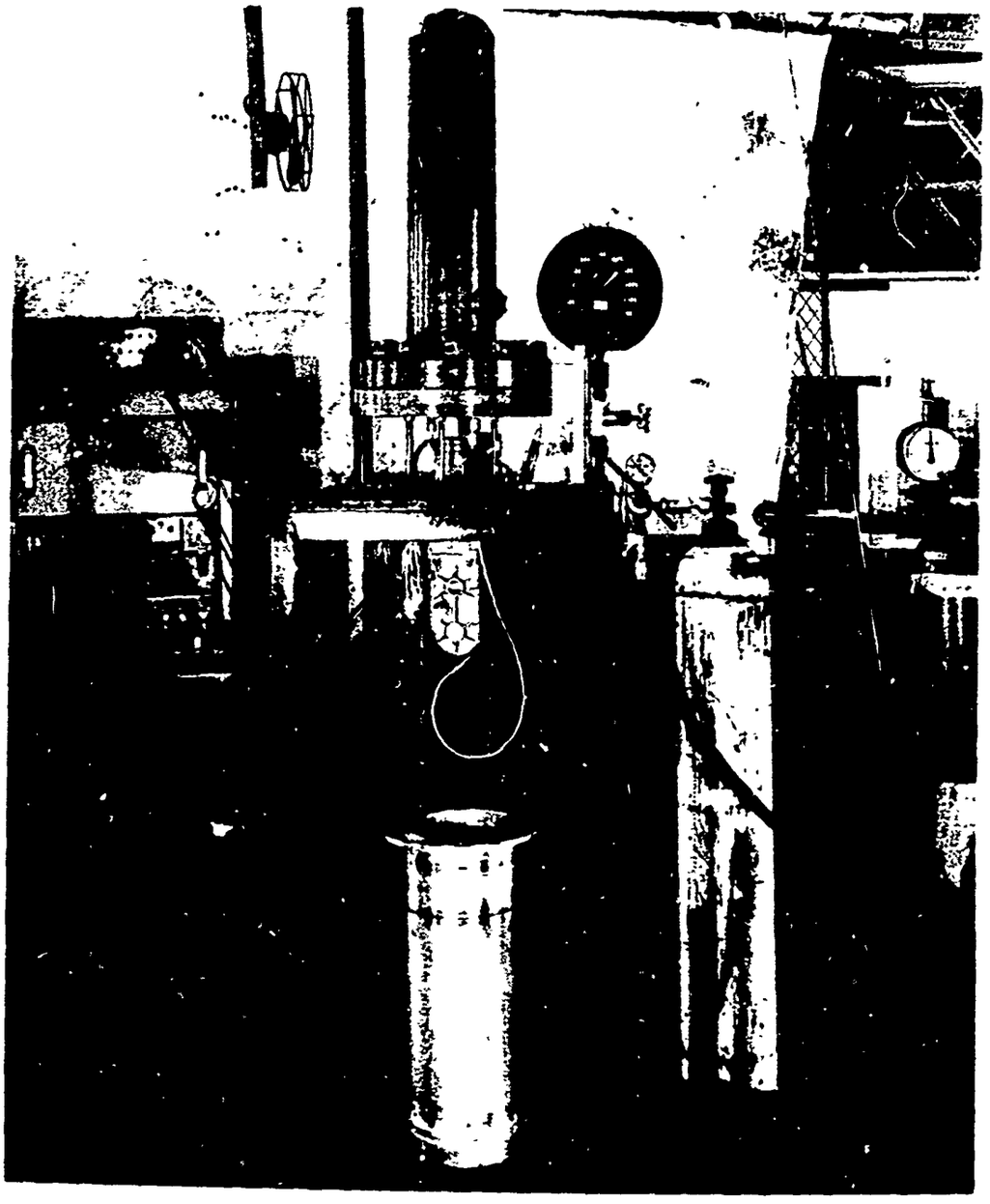

FIGURE 2.1

EXPERIMENTAL APPARATUS

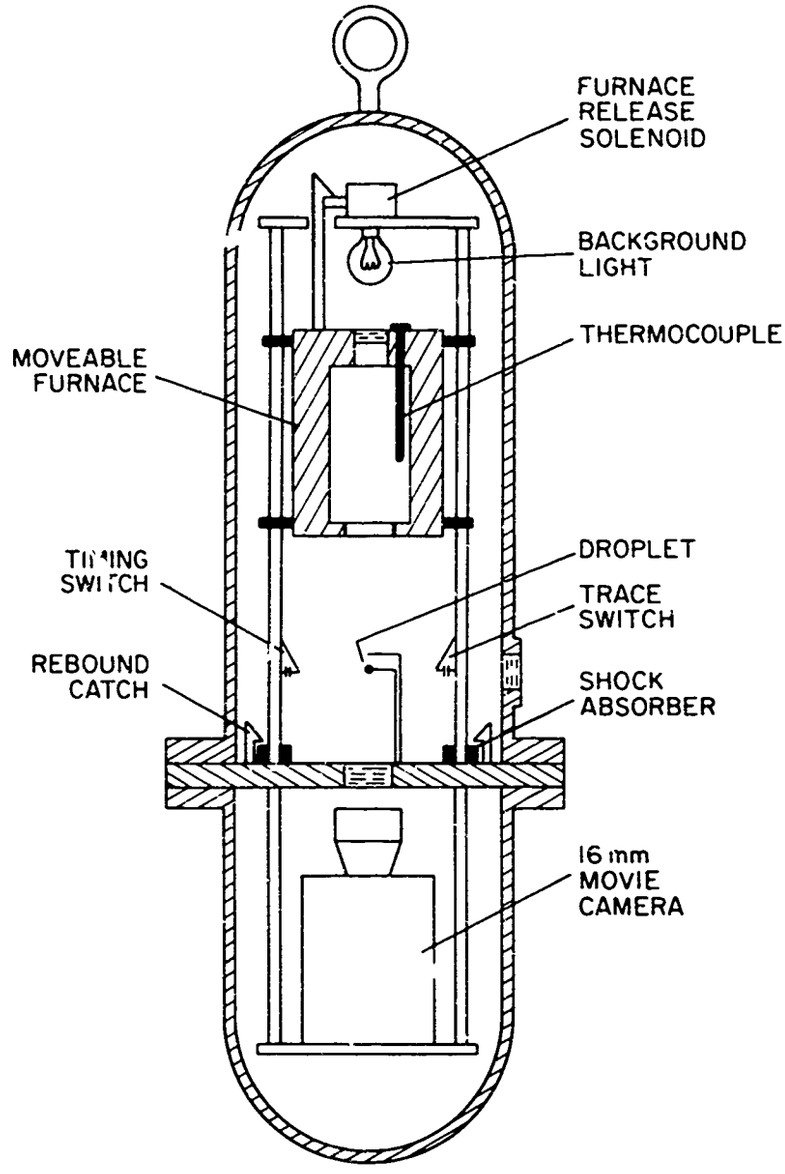

FIGURE 2.2

INTERNAL ASSEMBLY

5 atmospheres was made with an Ashcroft laboratory gauge with 1/2 PSI subdivisions. For tests above 5 atmospheres, an Ashcroft gauge with 50 PSI subdivisions was used. Commercially pure nitrogen was used to pressurize the chamber. The monopropellant used in the testing program was propylene glycol dinitrate.

The droplet was supported on either a quartz filament or the bead of a thermocouple junction. A sketch of the mount assembly is shown in Figure 2.3. The thermocouple was constructed from chromel-alumel wire having an outside diameter of .003 inches. The somewhat enlarged thermocouple junction had an average diameter of between .008 and .016 inches.

When only one thermocouple was used, it's output was fed directly into the vertical terminals of a Model 130B Hewlett-Packard oscilloscope. A Dumont, Type 2614, oscilloscope camera employing Type 47 Polaroid film was used to record the trace. In the dual thermocouple arrangement, the thermocouple outputs were fed into the terminals of two galvanometers in a Consolidated Electrodynamics Corporation Model 5-124 recording oscillograph. The quartz filament-single thermocouple arrangement was used primarily in the larger droplet sizes (.060 - .080 in.) because the small thermocouple junction could not support the large droplets.

The furnace consisted of a heating coil wound between an outer stainless steel cover and an inner ceramic core. The furnace was cylindrical in shape with an inside diameter of 2 in. and an

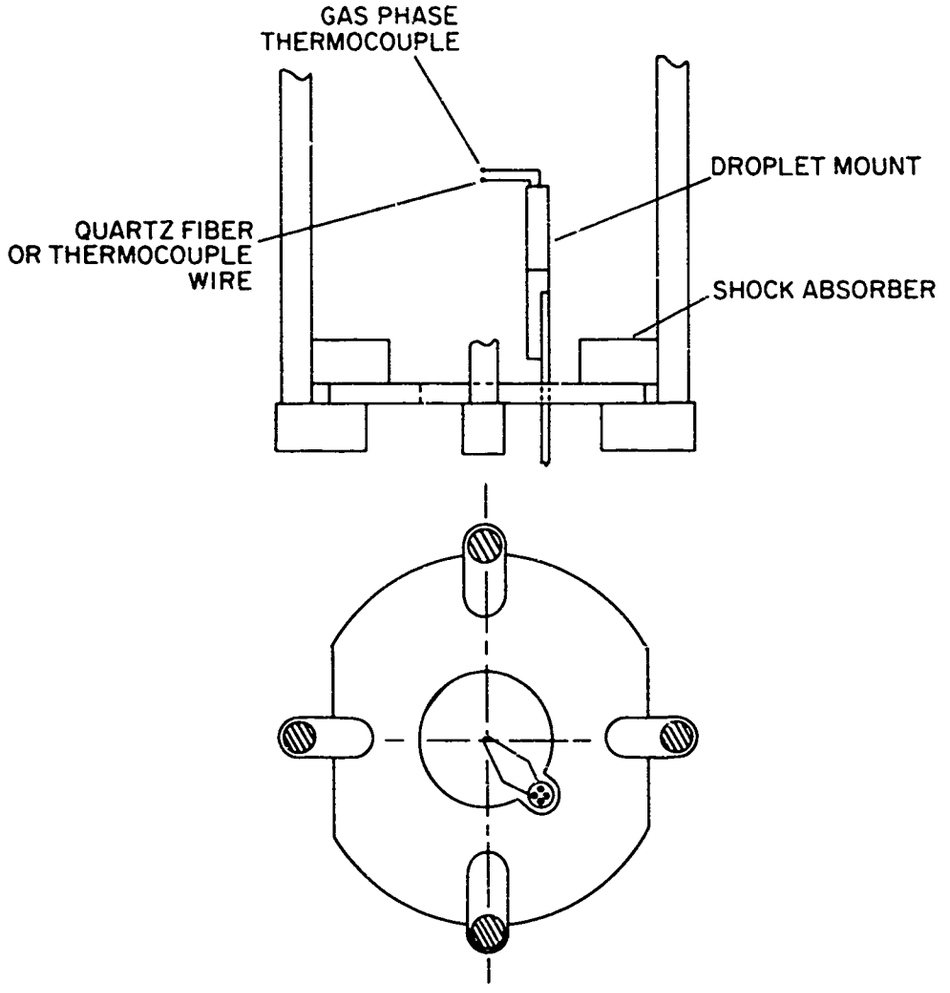

FIGURE 2.3

DROPLET MOUNT ASSEMBLY

outside diameter of 3-1/2 in. The over-all height of the furnace was 6-1/2 in. with an actively heated inside length of 5 in.

After the furnace was heated to the desired temperature, a solenoid was energized releasing it from its initial position. The furnace slid down guide rods to the droplet location where it was locked in place by two latches, thus providing rapid immersion of the droplet into the high temperature media. The time required for the furnace bottom to travel from the droplet location to the latches was about 50 ms. The shock of the fall was absorbed by two pieces of Resilite mounted on a false base. Resilite is an energy absorber sometimes used in athletic equipment to reduce shock. The Resilite shock absorbers combined with the latching mechanism eliminated extraneous motion of the gas around the droplet during the test period.

The bottom of the furnace was open, while the top was closed with a quartz window. This window allowed the passage of background illumination for photographic purposes, while preventing the escape of high temperature gas from the furnace into the chamber.

The gas temperature within the furnace was measured with a 1/8 in. O.D. sheathed chromel alumel thermocouple The thermocouple junction was located in a position that would correspond to the droplet position when the furnace was locked in place. This was about 2-1/2 in. from the base of the furnace. The

temperature indicated by this thermocouple just before each test was taken as the test temperature. The thermocouple was allowed to stabilize at a constant temperature before each test to insure a uniform furnace temperature.

The droplet was photographed through a quartz window in the base of the chamber using a 16mm Fastair missile camera. Kodak Tri-X negative film was used in the camera at a speed of approximately 80 frames per second. The background light was a small incandescent lamp. This illumination passed through the quartz window in the top of the furnace giving a shadowgraph of the droplet. A neon timing light in the camera allowed synchronization of the motion picture film and the oscilloscope trace. As the furnace reached the droplet location, it closed two switches which simultaneously completed the circuits of the timing marker and the oscilloscope trace, thereby indicating the beginning of the heat-up process.

2.2 Operation of the Apparatus

The over-all operation of the apparatus is illustrated in Figure 2.4. Conditions within the chamber at the beginning of a test are represented in the first diagram of Figure 2.4. At this point the furnace temperature has stabilized, the droplet has been placed on its support, and the chamber has been closed and pressurized. The background light has been turned on and the camera is off.

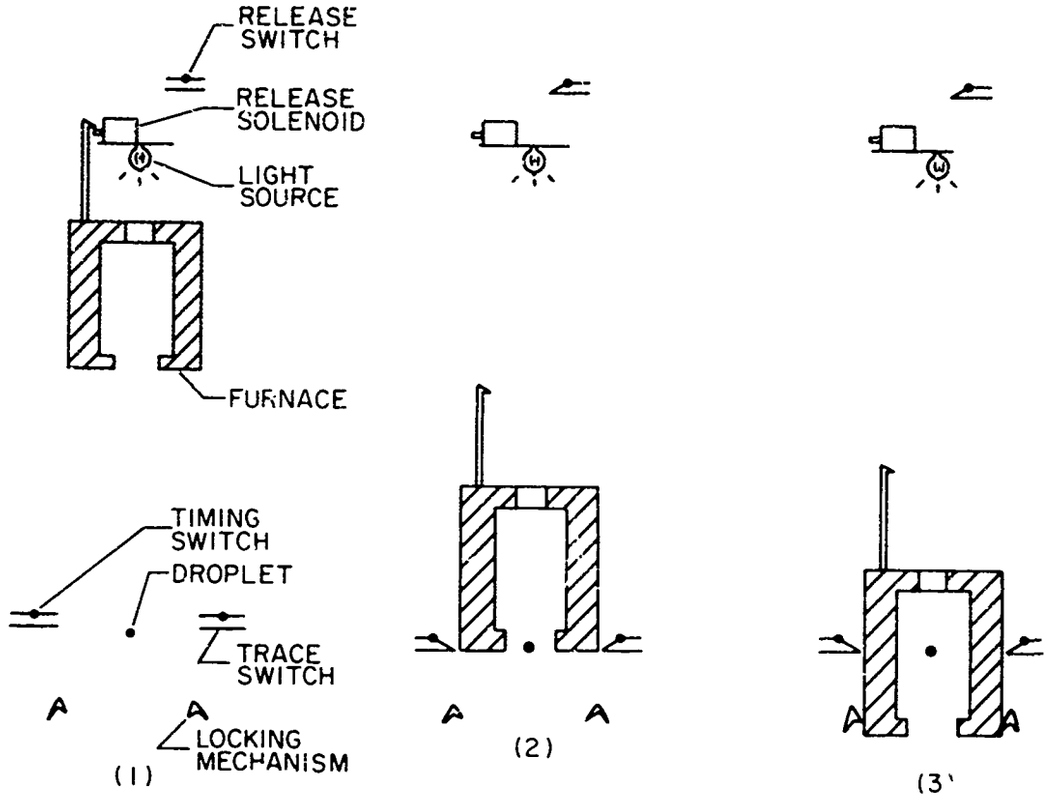

FIGURE 2.4

SEQUENCE OF OPERAT

To begin operation the oscilloscope sweep was triggered, the camera was started, and the furnace release solenoid was actuated allowing the furnace to fall. In the second diagram of Figure 2.4, the bottom edge of the furnace is just passing the droplet location. At this point the furnace closed two switches which simultaneously completed the oscilloscope trace circuit and the timing light circuit on the camera.

The third diagram of Figure 2.4 shows the furnace in its final locked position at the droplet location.

CHAPTER 3

IGNITION

3.1 Preliminary Results

The exact nature of the ignition process of a particular fuel varies with the chemical composition, environment, etc of the fuel being investigated. Consequently, preliminary experimental tests seemed advisable to assist in the selection of the ignition model. Typical results of these and later tests are shown in Figures 3.1 and 3.2.

Figures 3.1a and 3.1b which present data at 1 atm. total pressure over the experimental temperature range demonstrate a correlation between the beginning of diameter change and an inflection point in the liquid phase thermocouple record. The diameter change is the point in the diameter versus time plot where the diameter begins to decrease rapidly. It occurs very slightly before, or about the same time as the inflection point. A gas phase thermocouple was then introduced to indicate when a flame appeared in the gas phase, since the flame was not visible at low pressures. It is seen that the inflection in the gas phase thermocouple, which indicates the presence of a flame, exhibits the same correlation with the diameter change that the liquid

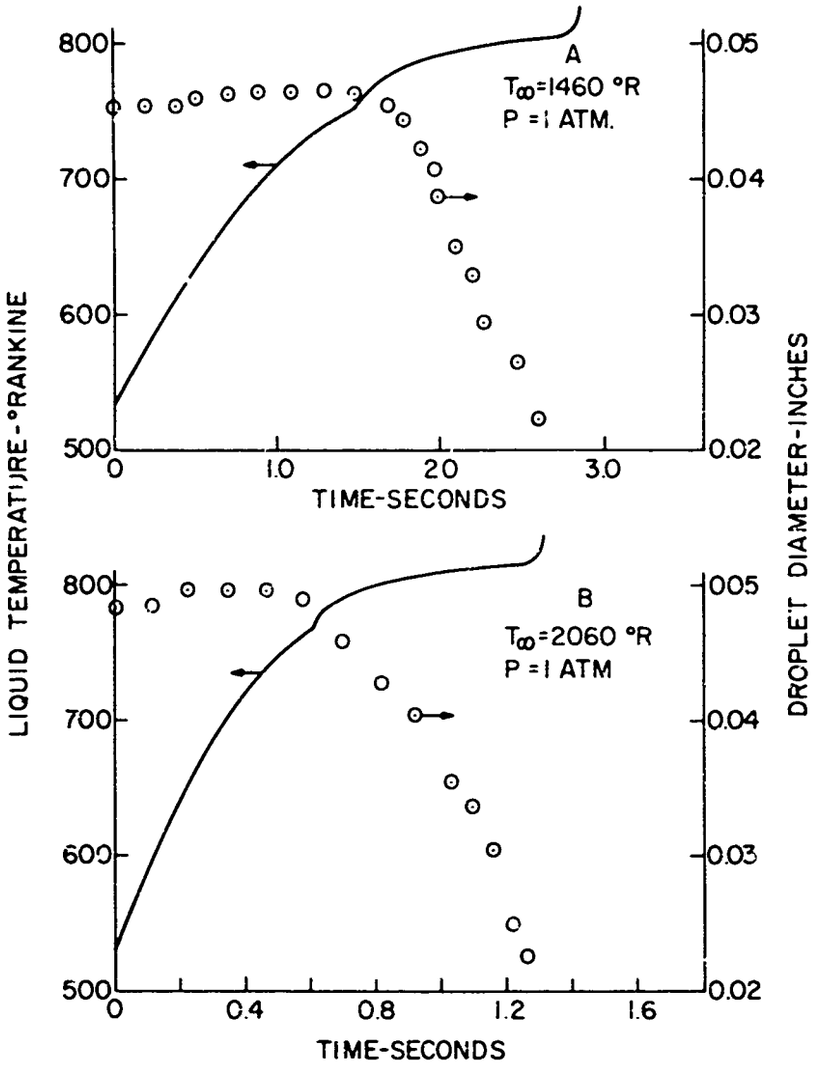

FIGURE 3.1

IGNITION AT VARIOUS TEMPERATURES

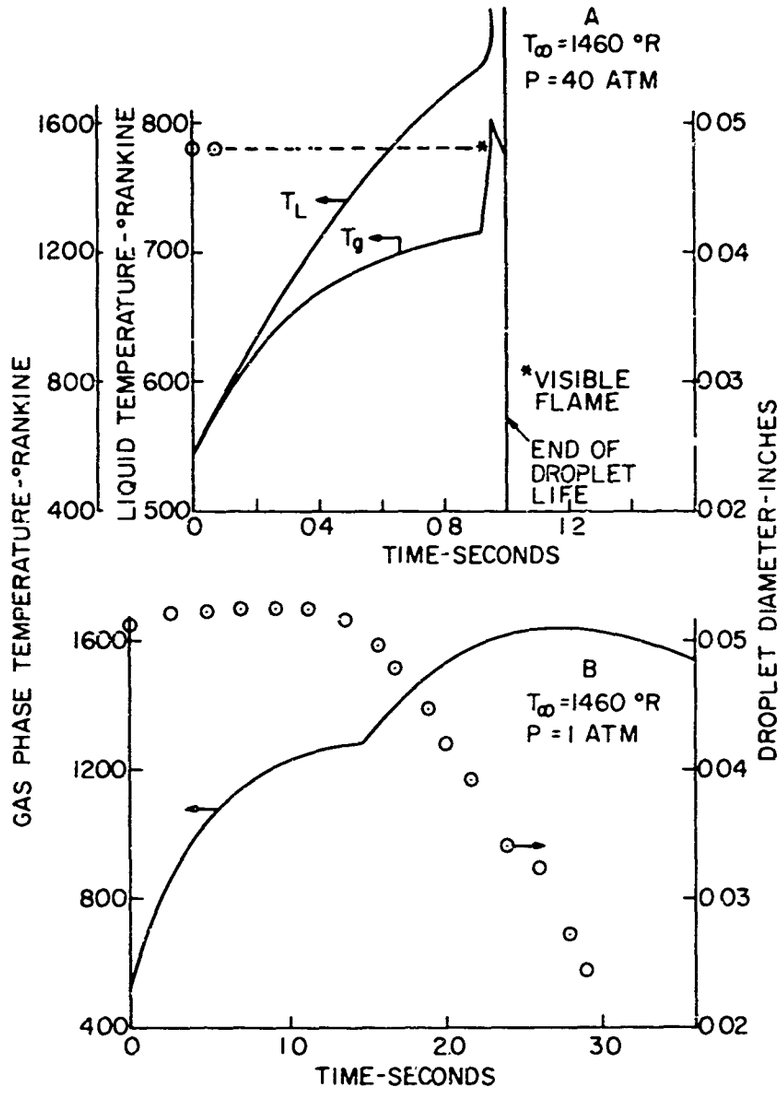

FIGURE 3.2

IGNITION AT VARIOUS PRESSURES

thermocouple had, as evidenced in Figure 3.2b. That is, the liquid and gas traces inflect at the same time, or very slightly after, the diameter change occurred. This correlation extends over the entire test range. Figure 3.2a, which presents data at 40 atmospheres pressure, shows excellent agreement between the inflections of the two curves and the appearance of the luminous flame. The diameter of the droplet during the pre-ignition period could not be measured accurately at high pressures, due to the scattering of the background light rays by natural convection patterns on the furnace window.

On the basis of the preceding information, a criterion for the ignition time was established. Each acceptable data point had to have at least two separate indications of ignition that occurred at very nearly the same time. Gas or liquid thermocouple inflection and diameter change or, at high pressures, gas or liquid thermocouple inflection and luminous flame were the combinations used.

Figures 3.3 and 3.4 show sample photographs of the ignition and combustion processes. They illustrate the extremes of the problem of ignition identification. In Figure 3.3, where the visible flame was used as the ignition indicator, the film record between .31 and .85 seconds was eliminated since no significant changes in the droplet were observed during that period. Note how the natural convection patterns on the furnace window in

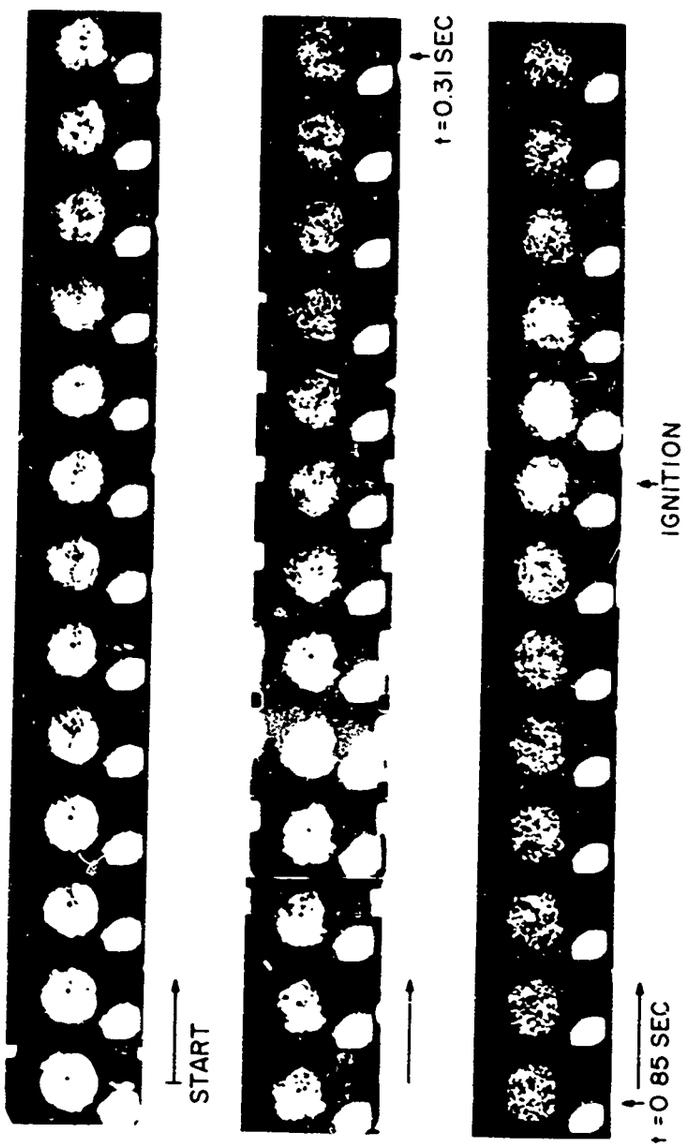

FIGURE 3.3

SAMPLE PHOTOGRAPH - VISIBLE FLAME

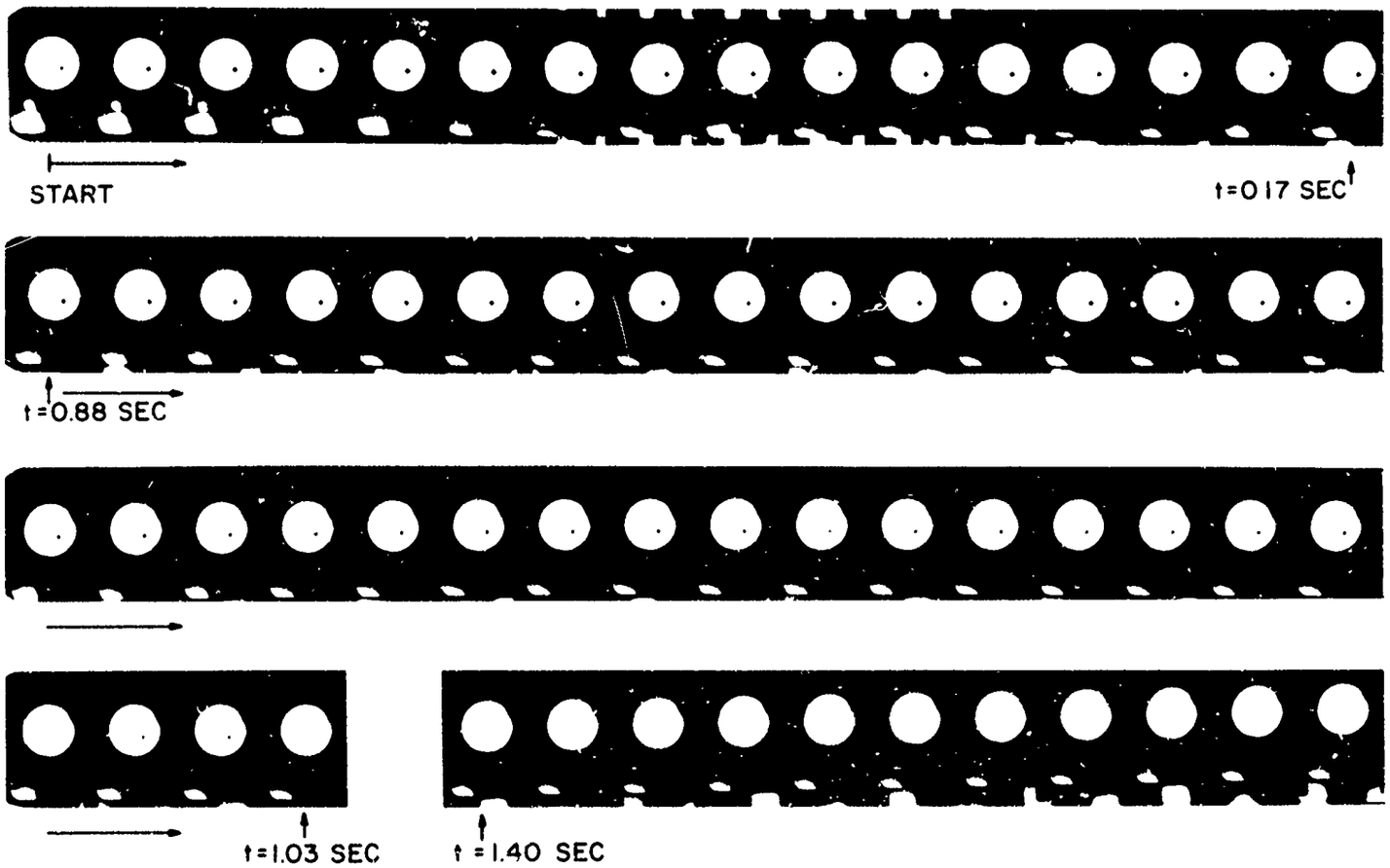

FIGURE 3.4

SAMPLE PHOTOGRAPH - FLAME NOT VISIBLE

Figure 3.3, at 40 atmospheres total pressure, tend to obscure the droplet during the pre-ignition period. No such problem was encountered in the 1 atmosphere test of Figure 3.4. The droplet remained essentially unchanged between .17 and .88 seconds, so this film was excluded. Shortly after .88 seconds the droplet begins to steadily decrease in size until it is almost completely consumed at 1.03 seconds. The empty probe is all that remains at 1.40 seconds. As noted by other experimenters,[3,7,12] the droplet is not exactly spherical during the test period. To retain a degree of uniformity with previous workers in the field, the droplet was assumed to have the shape of an ellipsoid. The diameter of the droplet was then defined to be the diameter of a sphere having a volume equal to the volume of the ellipsoid.

The equivalent sphere's diameter is related to the minor and major axes, ℓ_1 and ℓ_2, of the ellipsoid by the equation

$$D = (\ell_1^2 \ell_2)^{1/3} .$$

Upon examining the behavior of the droplet in Figure 3.1, a gradual increase in the rate of decrease of the droplet diameter may be observed after ignition has occurred. Two possible causes of this are the increased strength of the flame as the burning process progresses and the increased mass transfer rates at high vapor pressures, irrespective of flame location.

The liquid temperatures of the droplet of Figure 3.1 apparently begin to heat up to a wet bulb temperature consistent with the temperature of the environment. However, when ignition occurs the droplet sees the higher temperature of the flame zone and its temperature then rises to an equilibrium temperature in the presence of the flame.

3.2 Theoretical Considerations

On the basis of these preliminary tests, two theoretical models were developed to describe the pre-ignition behavior of a motionless droplet instantly surrounded by a high temperature inert atmosphere. The following assumptions were made in the analysis:

1. The droplet is composed of a single chemical species.
2. In the first model the droplet temperature is assumed uniform, but varying, while the second model considers transient temperature gradients in the droplet.
3. Properties are constant in both the liquid and gas phases.
4. No surface evaporation occurs, and the droplet radius remains constant.
5. The heat transfer and diffusion processes are spherically symmetrical.
6. The influence of mass transfer on the heat transfer characteristics of the boundary layer around the droplet is neglected.

7. Since ignition occurred when the droplet temperature approached the wet bulb temperature, which is relatively near to the boiling point at the total pressure of the test, it appeared reasonable to take the time required for a droplet to heat up to the boiling point as an estimation of ignition time.

Considering first the uniform temperature, or infinite conductivity, model, the energy equation is

$$\sigma B(T_\infty^4 - T^4)A + hA(T_\infty - T) = \rho C_p V\frac{dT}{dt} \qquad 3.1$$

assuming $T_\infty^4 \gg T^4$, Equation 3.1 may be integrated directly to yield

$$t = \frac{\rho C_p D_o^2}{6Nuk_g} \ell n \left[\frac{1 + \dfrac{Nuk_g}{\sigma B D_o T_\infty^4}(T_\infty - T_c)}{1 + \dfrac{Nuk_g}{\sigma B D_o T_\infty^4}(T_\infty - T_\cdot} \right]. \qquad 3.2$$

The Nusselt number is determined by employing the results of Ranz and Marshall[20] for natural convection heat transfer to drops.

$$Nu = 2.0 + 0.6\, G_R^{0.25}\, P_R^{0.33}$$

Consider now the finite conductivity case with temperature gradients existing in the droplet. In this analysis the complete energy equation must be considered within the droplet. It is assumed in the formulation that radiation is absorbed uniformly throughout the droplet. This assumption seems realistic for droplets of the sizes studied in view of the theoretical considerations by Hottel et al[9] on droplet radiation absorption characteristics. Since $T_\infty^4 \gg T^4$, the surface radiation flux is taken as $\sigma B T_\infty^4$ and the radiation absorbed per unit volume is

$$Q = \frac{3\sigma B T_\infty^4}{r_o} \qquad 3.4$$

The energy equation within the droplet for the finite conductivity case becomes:

$$\rho C_p \frac{\partial T}{\partial t} = k \frac{1}{r^2} \frac{\partial}{\partial r} \left(r^2 \frac{\partial T}{\partial t} \right) + Q \quad . \qquad 3.5$$

The boundary conditions available for the solution of the energy equation are the surface convection condition, and the existence of a finite solution at the droplet center.

$$k \frac{dT}{dr} = h(T_\infty - T), \quad r = r_E \qquad 3.6$$

T is finite, $r = 0$

The equations were first put in dimensionless form by the following substitutions:

$$\theta = \frac{T - T_o}{T_\infty - T_o}$$

$$\eta = r/r_o$$

$$\tau = \frac{kt}{\rho C_p r_o^2}$$

With these substitutions, Equation 3.5 becomes

$$\frac{\partial \theta}{\partial \tau} = \nabla^2 \theta + \psi \qquad 3.7$$

Where,

$$\psi = \frac{Q r_o^2}{k(T_\infty - T_o)}$$

and the non-dimensionalized boundary conditions are:

$$\frac{\partial\theta}{\partial\eta} = \frac{Bi}{2}(1 - \theta), \quad \eta = 1$$

$$\theta \text{ is finite}, \quad \eta = 0 \quad .$$

The Laplace transform method was used to solve Equation 3.7 with the boundary conditions of 3.8. The complete details of the solution may be found in Appendix A. The solution for the temperature distribution in the sphere as a function of time with convection and radiation heating is

$$\theta = 1 - \frac{Bi}{\eta} \sum_{n=1}^{\infty} \sqrt{\frac{Y_n^2 + \left(\frac{Bi}{2} - 1\right)^2}{Y_n^2 + \frac{Bi}{2}\left(\frac{Bi}{2} - 1\right)}} \frac{\sin(Y_n\eta)}{Y_n^3} \cdot \left[Y_n^2 e^{-Y_n^2\tau} - \psi\left(1 - e^{-Y_n^2\tau}\right)\right]$$

where:

$$\tan Y_n = \frac{-Y_n}{\frac{Bi}{2} - 1} \quad .$$

This solution was evaluated on the IBM 7074 computer using the first five roots of Tan Y_n, as tabulated by Schneider[23], for various values of Bi and ψ.

The radiation absorption coefficient B, for both models was taken to be 0.5. On the basis of the experimental results of Faeth[7], and the theoretical work of Hottel, et al[9] this value seems realistic for the droplet sizes studied. Property values employed in the calculations may be found in Appendix B.

The effect of including radiation in the finite conductivity analysis is shown in Figure 3.5. At the surface of the droplet, the temperatures predicted by the finite conductivity model with no radiation are 15 to 20 per cent below the temperatures of the model that included radiation. Since the surface temperature is of primary importance in determining the theoretical ignition delay time, it is apparent that radiation should be included. Figure 3.5 also indicates that significant temperature gradients exist in the droplet. The importance of this is recognized in relation to the liquid phase thermocouple readings. Since the thermocouple is located at some point in the droplet between the center and the outer edge, it will indicate a temperature somewhat below the actual surface temperature.

Finally, the temperature at which ignition occurred was assumed to be the boiling temperature of the fuel droplet. The boiling temperatures were determined by employing the vapor pressure data of Beilstein[4] and de C. Crater[6] for propylene glycol dinitrate between 10^{-5} and 10^{-1} atms. Reid and Sherwood[21] indicate that a plot of ln P_{vp} versus 1/T usually gives a reasonably straight

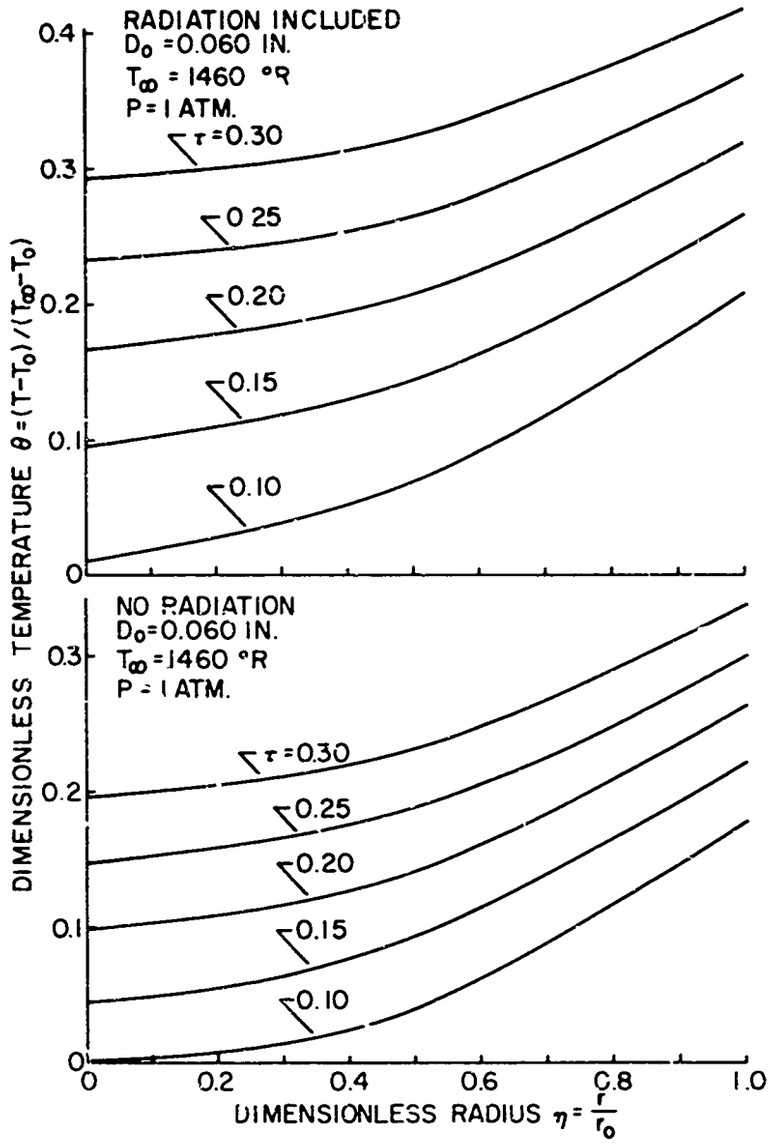

FIGURE 3.5

FINITE CONDUCTIVITY MODEL

line. By fitting a straight line through the data available, and extending it, at constant slope, to higher pressures, the boiling temperatures were obtained at those pressures The straight line assumption of Figure 3 6 seems reasonable in view of Figure 3.7. All three compounds plotted using Lange's[14] data exhibited the straight line characteristic up to the critical point.

3.3 Experimental Results and Discussion

In order to evaluate the suitability of the proposed ignition models, further tests were conducted. The results of the experimental program are presented in Figures 3 8 through 3.12

Figure 3 8 presented the variation of ignition delay time with initial droplet diameter at a total pressure of 1 atmosphere and an ambient temperature of 1460^{c}R Although the infinite conductivity model is in rough agreement with the data, the finite conductivity model gives a superior fit of the trends of this figure However, due to the approximate nature of the models and the inaccuracies due to series truncation of the finite conductivity model for small times, it seems sufficient to base the comparison on the infinite conductivity model

The variation of ignition delay time with ambient temperature for a given droplet size is presented in Figure 3 9 Again the analysis follows the general trend of the experimental results reasonably well. The change in ignition delay is explainable by faster heat-up rates at higher ambient temperatures This indicates

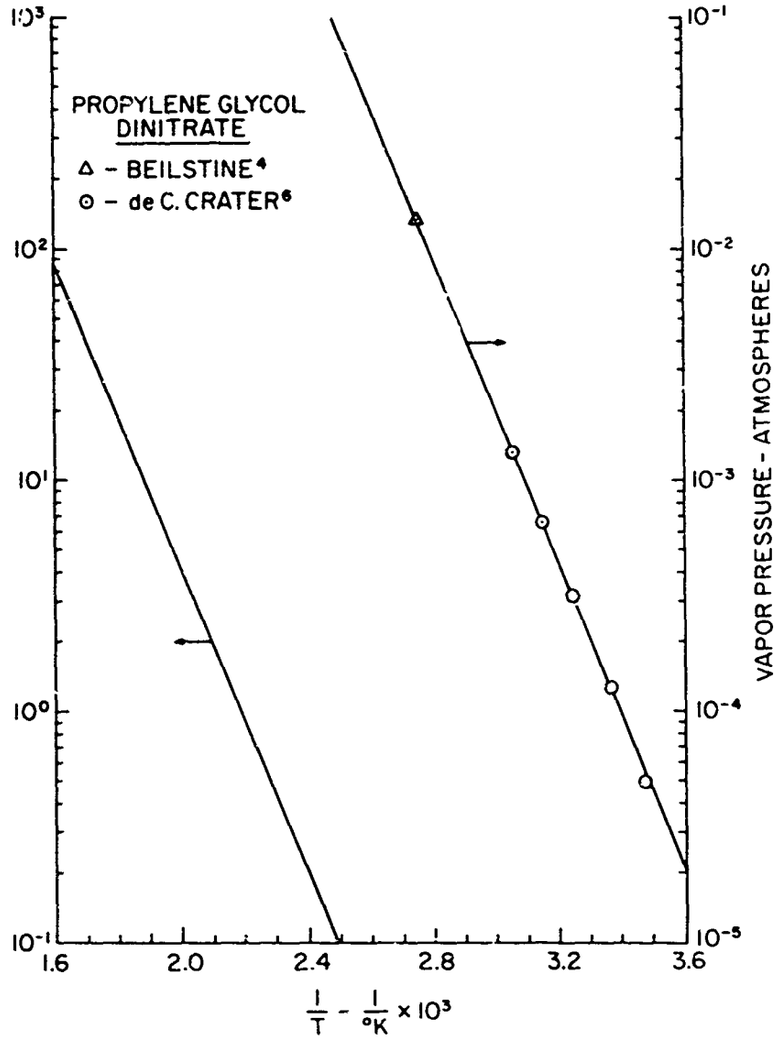

FIGURE 3.6

VAPOR PRESSURE ASSUMPTION

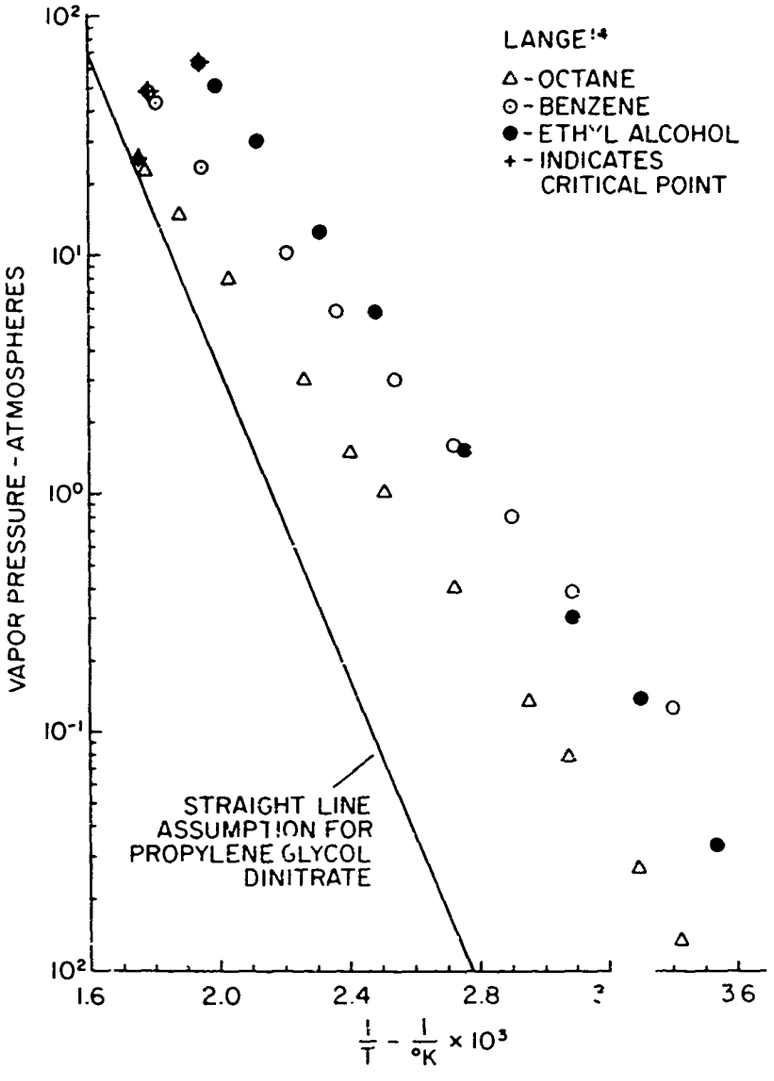

FIGURE 3.7

VAPOR PRESSURE DATA

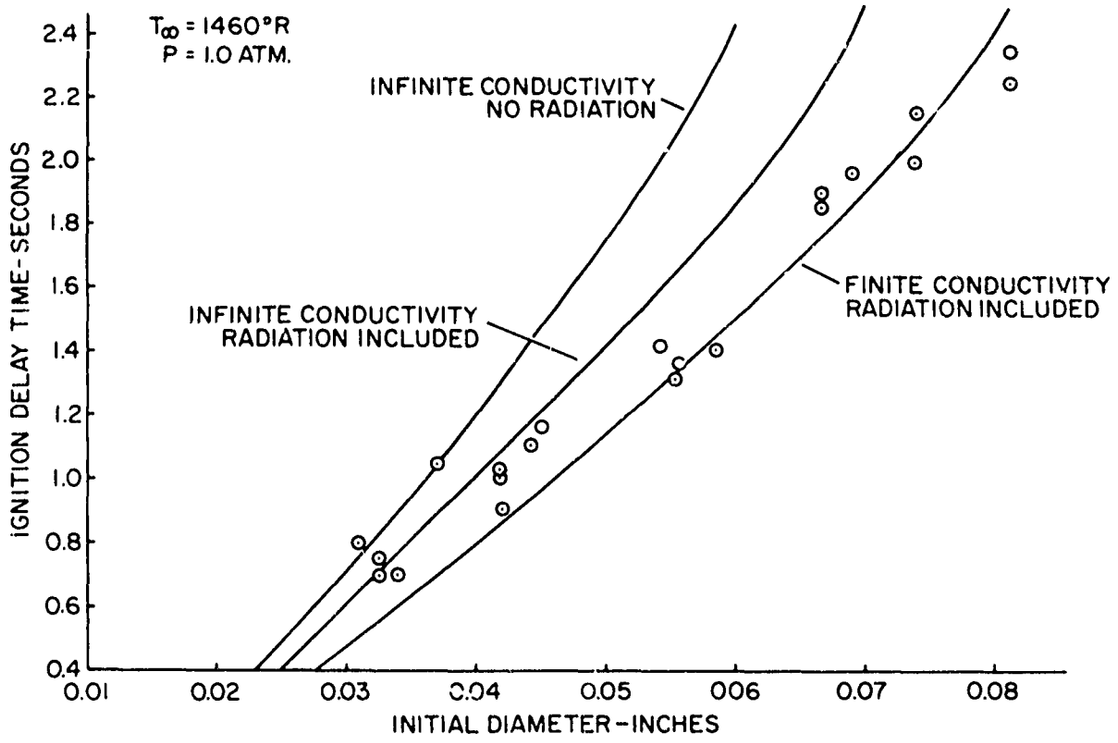

FIGURE 3.8

IGNITION DELAY AT VARIOUS INITIAL DIAMETERS

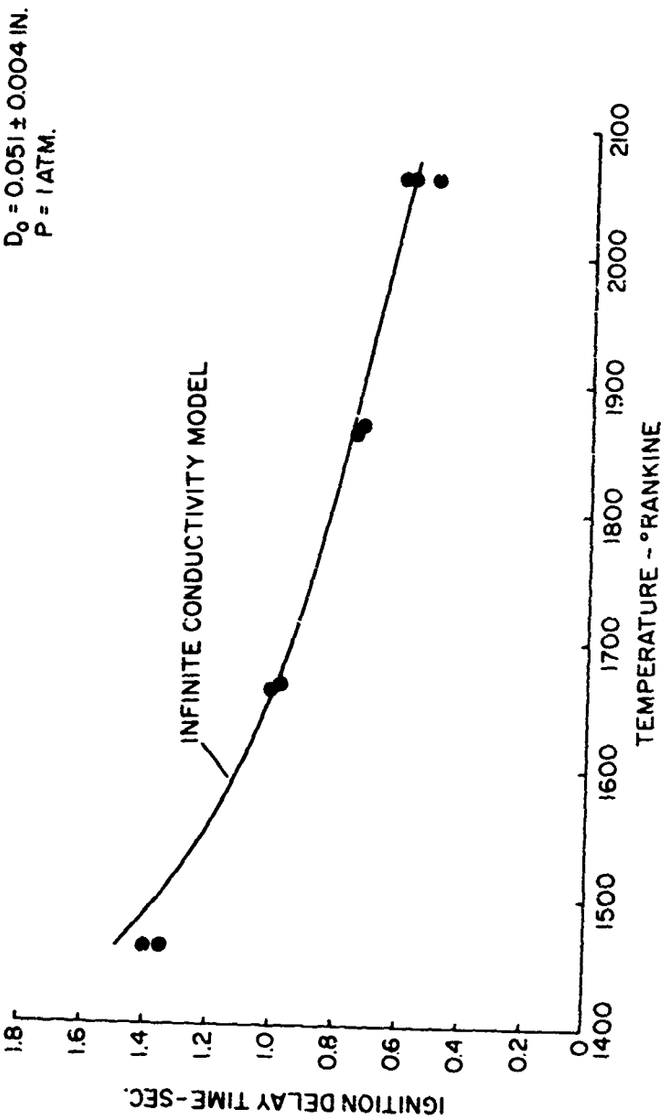

FIGURE 3.9

IGNITION DELAY AT VARIOUS AMBIENT TEMPERATURES

that ambient temperature exerts primary influence on heat-up rates at this pressure, rather than pre-ignition chemical kinetics as is the case for bipropellant ignition.[7]

Finally, the effect of various total pressures on the ignition delay time is presented in Figure 3.10 and 3.11. As the ambient temperature increases, the data follows the analysis more closely at low pressures. However, above 1 atm. total pressure the analysis appears to break down somewhat. Considering Figure 3.11, it may be noted that in all three cases the temperature indicated by the liquid thermocouple falls between the center and surface temperatures of the finite conductivity model. From the 0.1 atm and 1 atm data, it appears reasonable to assume that ignition occurred at a temperature reasonably close to the wet bulb, or boiling temperatures predicted by Figure 3.7 However. the ignition temperature of the 11 atm test appears to be far from the 1060^{o}R temperature estimated from Figure 3.7. Figure 3.12 shows that, in the lower temperature range, the maximum measured liquid temperature compares reasonably with the boiling temperature determined from the vapor pressure curve. However, above 1 atmosphere there is a marked departure from the curve. It is possible that ignition did not occur at the boiling temperature, but, more accurately, at the wet bulb temperature for a given pressure. While the wet bulb and boiling temperatures roughly correspond at low pressures, this is not necessarily the case at high pressures.

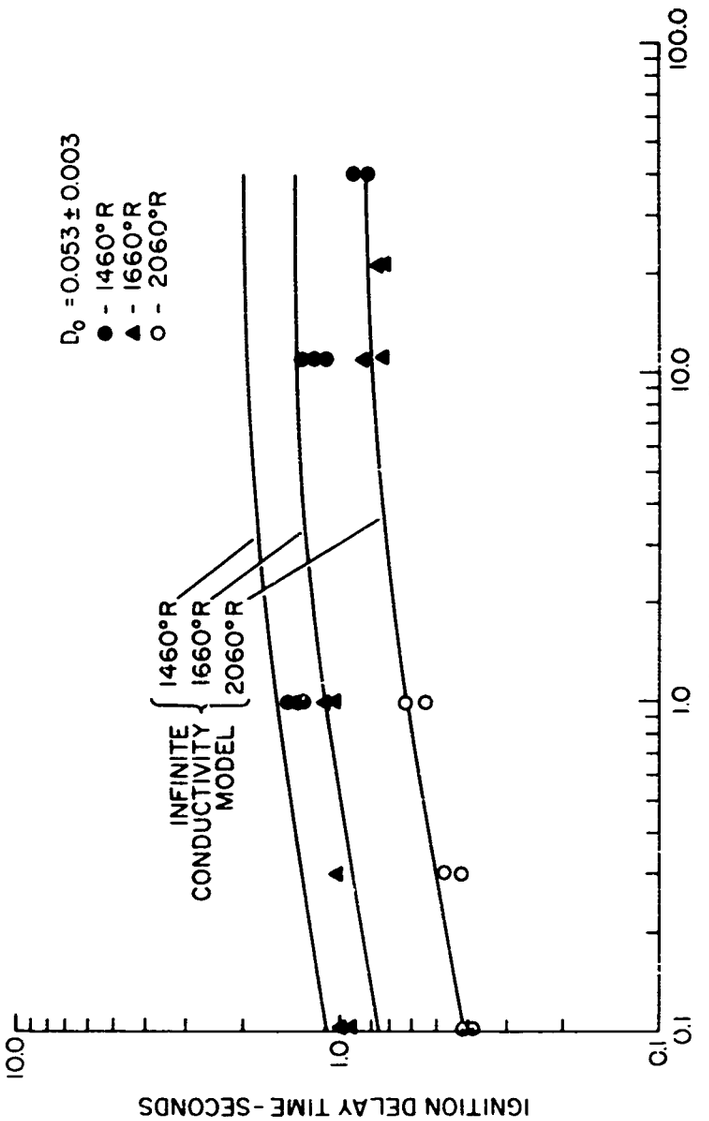

FIGURE 3.10

IGNITION DELAY AT VARIOUS PRESSURES

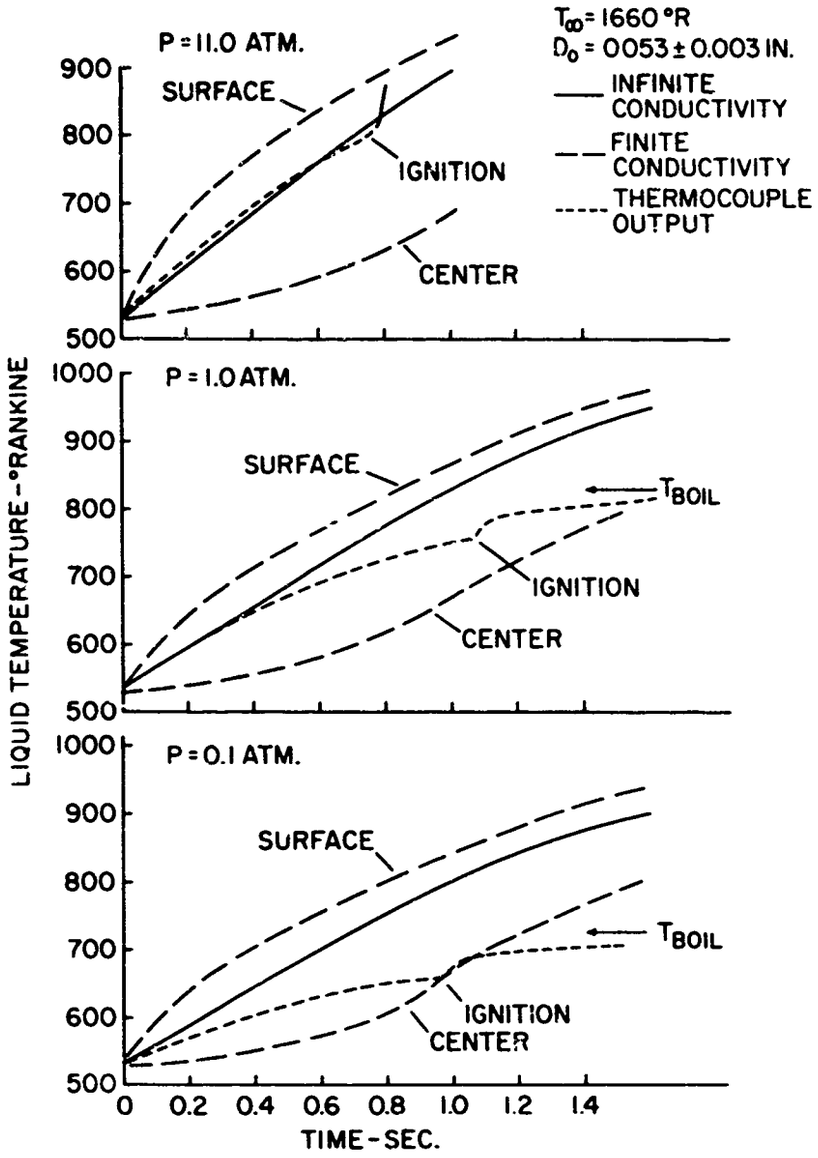

FIGURE 3.11

LIQUID TEMPERATURE AT VARIOUS PRESSURES

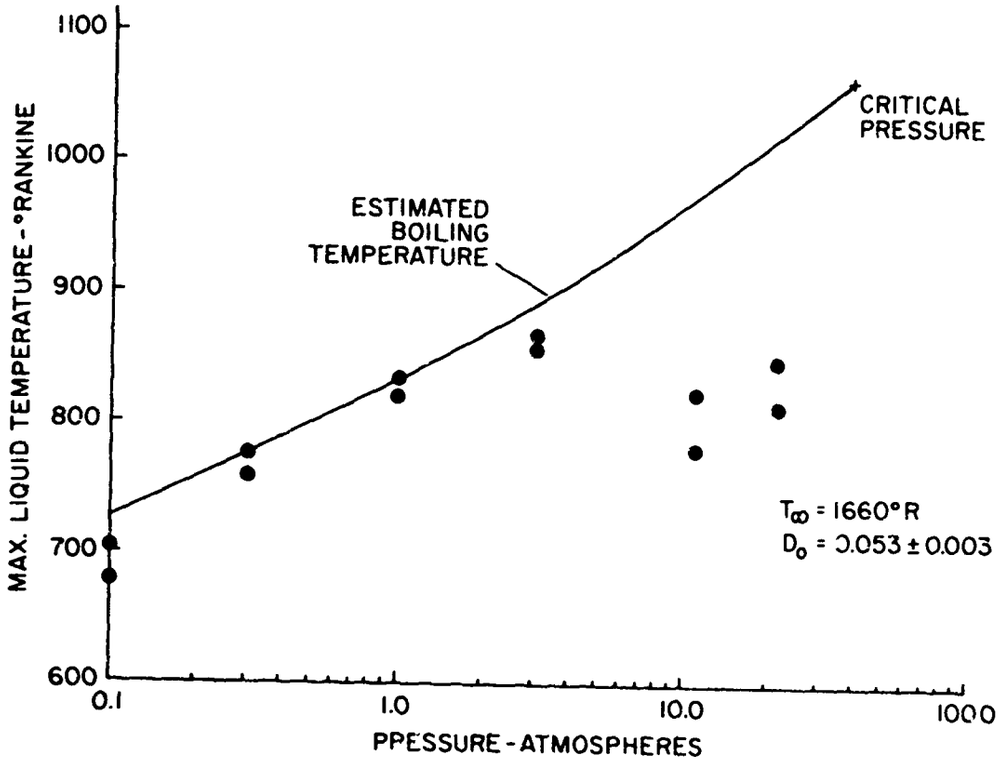

FIGURE 3.12

LIQUID TEMPERATURE ASSUMPTION

Also, it is important to note that in none of the data at 10 atmospheres and above was a steady state burning condition attained. Apparently the flame becomes strong enough to increase reaction rates even when fuel concentrations are below those which would be attained at the wet bulb condition. Thus, the burning lifetimes of the droplets in this pressure range were very small in comparison to the heat-up time, and the combustion process did not occur at a uniform temperature.

CHAPTER 4

COMBUSTION

4.1 Theoretical Considerations

The burning rate, or mass of material per second leaving a droplet, can be written from a simple mass balance, as

$$\dot{m} = \frac{d}{dt}\left(\frac{\pi}{6} D^3 \rho\right); \qquad 4.1$$

assuming constant density

$$\dot{m} = \frac{\pi}{6} \rho \frac{d(D^3)}{dt} \qquad 4.2$$

For bipropellant diffusion flames $dD^2/dt = -C$ (a constant). This D^2 correlation was used by Barrere and Moutet[3] in their study of other monopropellants, so in order to compare results this data was correlated in a similar manner. It is recognized from the results of Williams[26] that the D^2 relation is not strictly valid for monopropellant flames. However, due to the limited experimental diameter range it was difficult to distinguish whether dD/dt = const., or dD^2/dt = const , or whether some intermediate case existed. Using the D^2 correlation, Equation 4.2 becomes

$$\dot{m} = -\frac{\pi}{4} \rho D C \qquad 4.3$$

where C is known as the burning rate constant during the quasi-steady state burning period. The value of C for a particular combustion process is obtained from the slope of the D^2 versus time plot during the burning period. However, since the droplet diameter, D, is constantly decreasing during the burning period, Equation 4.3 is valid at any instant in the burning period. Therefore, to obtain a mass burning rate from the data available, it was necessary to define $\bar{D}$ as the average droplet diameter during the quasi-steady state burning period

$$\dot{m} = -\frac{\pi}{4} \rho \bar{D} C \qquad 4.4$$

The problem of predicting the mass burning rates of mono-propellant droplets has been investigated analytically by several authors[8,22,24,26]. Since the analysis presented by Williams[26], for motionless droplets, involves measurements and properties readily available and can be applied to non-adiabatic burning it appeared most useful for this study. The simplified model presented by Williams[26], and first attributed to Spalding[22] includes the following assumptions:

1. The activation energy is sufficiently large so that all heat release will occur in a thin shell at some distance from the droplet surface.
2. The droplet temperature is constant
3. The flame is spherically symmetrical and natural convection is neglected
4. Thermal diffusion is neglected
5. Quasi-steady burning is considered.
6. All gases obey the ideal gas equation of state, and the total pressure is constant

The equations presented by Williams[26] are

$$\ell n\,[1 + (T_c - T_E)/\lambda T_\infty] = (\dot{m}C_p/4\pi r_E k)_{r_c} - 1/r_c \qquad 4.5$$

$$T_c/T_\infty = T_E/T_\infty - \lambda + q - (1 - T_E/T_\infty - \lambda + q)\exp[-(\dot{m}C_p/4\pi r_E k)_{r_c}] \qquad 4.6$$

$$\sigma_c = (\dot{m}/4\pi r_E^2 \rho_c v_c)^2 \qquad 4.7$$

The unknowns in the above equation are T_c, $\dot{m}_{r_c}$, and $\rho_c v_c$. However, from a strictly phenomenological approach to the combustion process, assuming a first order reaction with one step kinetics

$$\rho_c v_c \propto p^N \text{EXP}\left\{ - \frac{E}{R_o T_c} \right\} \qquad 4.8$$

This is the additional relationship available to solve the system of equations.

The experimental and theoretical works of Phillips[18,19], Levy[15] and others[1,5] indicate that the gaseous decomposition of organic nitrates obeys the Arrhenius expression $K = X \text{ EXP}\left(-\frac{E}{R_o T_c}\right)$. The basic mechanism of decomposition is the breaking of the $O\text{-}NO_2$ bond. For propylene glycol dinitrate, as reported by Phillips[18], this process requires an activation energy of 37.4 $\frac{\text{kcal}}{\text{mole}}$. Thus, although the fuel obeys the first order law consistent with the analysis, its activation energy may not be sufficiently high to validate the thin flame assumption.

4.2 Experimental Results and Discussion

Figures 4.1 and 4.2 present the mass burning rates obtained by correlating the test data with Equation 4.3. The curves fitted through the points of Figures 4.1 and 4.2 indicate the general trends of the results and do not represent the predictions of an analytical model. The data of Figure 4.1 was found to be of the same numerical level as the data of Barrere and Moutet[3] for ethyl nitrate and propyl nitrate in the same temperature range. As may be noted in Figure 4.2, limited data was obtained at higher pressures. This was due to the fact that the luminous flame present

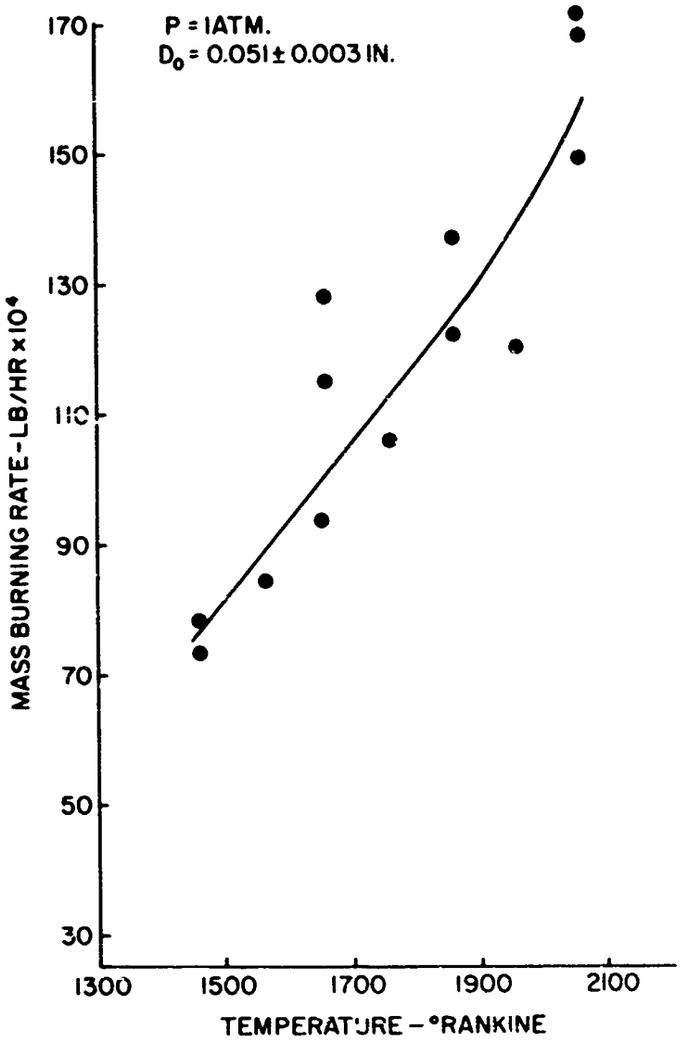

FIGURE 4.1

BURNING RATES AT VARIOUS AMBIENT TEMPERATURES

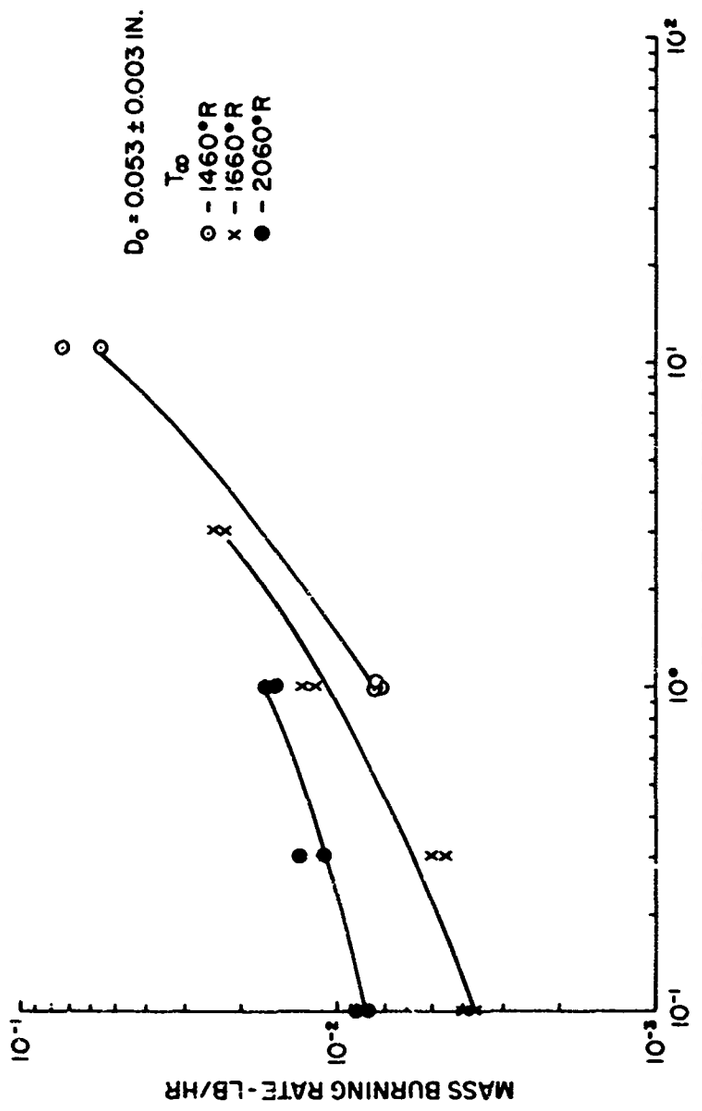

FIGURE 4.2

BURNING RATES AT VARIOUS TOTAL PRESSURES

in that region prevented measurement of the droplet during the burning period. Consequently, Equation 4.3 could not be evaluated. It should also be noted that quasi-steady state burning was not attained in the 11 atm results of Figure 4.2, as the droplet temperature was constantly increasing during the burning process. Had a new wet bulb temperature been maintained during the combustion process, the mass transfer rates would probably be higher. The general trend of the results of Figures 4.1 and 4.2 is for the burning rate to increase with increasing ambient temperature and pressure. This is consistent with Equation 4.8 since $\rho_c v_c$ may be thought of as a burning rate per unit area. However, it does not seem reasonable that the rapid change of the burning rates of Figure 4.1 can be explained by ambient temperature changes alone.

To compare the analysis presented by Williams[28], Equations 4.5, 4.6 and 4.7 were solved simultaneously on the IBM 7074 computer. The experimental mass burning rates were used for $\dot{m}$ and the three unknowns then were T_c, β_c, and $\rho_c v_c$. If the combustion process followed the analysis closely, it should be possible to determine the activation energy from a $\log \rho_c v_c$ versus $1/T_c$ plot and compare it with the previously measured activation energy of 37.4 $\frac{\text{kcal}}{\text{mole}}$[18]. This was done in Figure 4.3 for the variable temperature data of Figure 4.2, using various values for the thermal conductivity. It was found that it was necessary to use an unrealistically high value of the thermal conductivity to get an activation energy close to 37.4 $\frac{\text{kcal}}{\text{mole}}$. Other possible causes

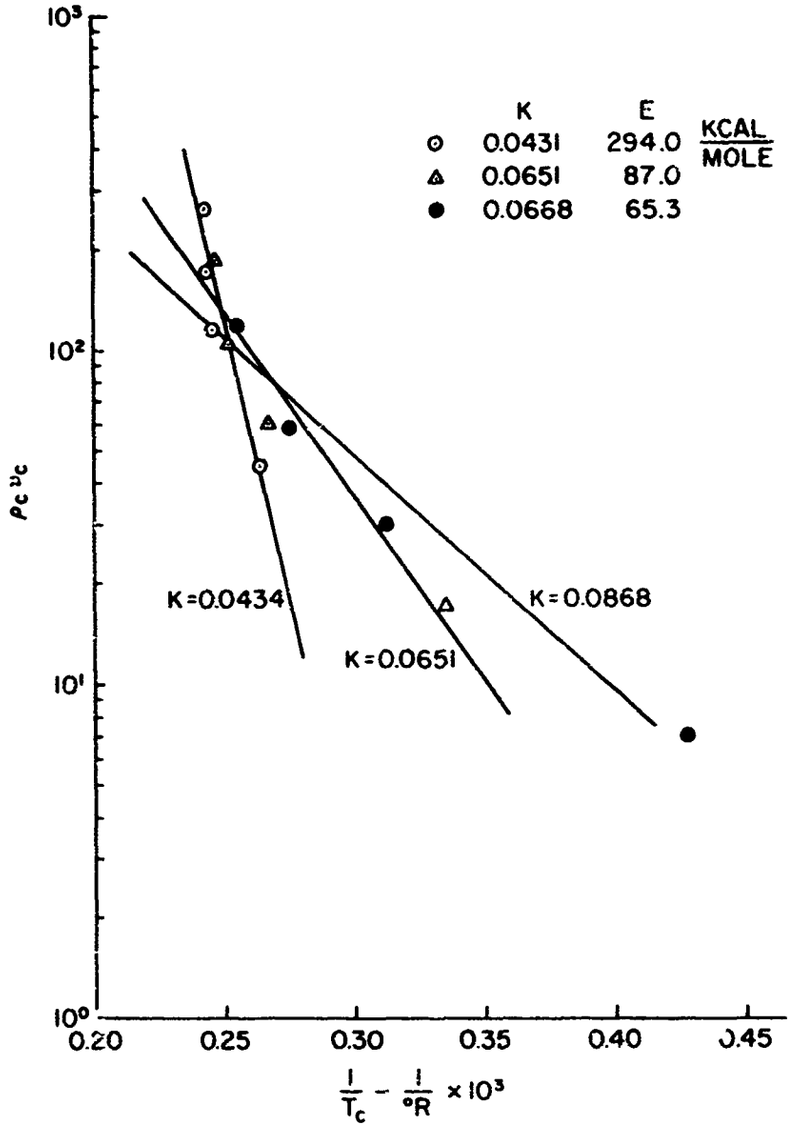

FIGURE 4.3

ACTIVATION ENERGY ASSUMPTION

of this deviation may be pointed out. First, as previously noted, the thin flame model of Williams may be in error. The more general case of a flame of finite thickness would result in a lower flame temperature and lower mass transfer rates. Also, it is important to note that adiabatic burning was not attained. Faeth's[8] analysis, which considers non-adiabatic burning, shows that the non-adiabatic boundary influences the burning rate of the droplet in several ways. First, the heat transported to the surroundings is not available to vaporize the fuel, and secondly, the reduced flame temperature decreases reaction rates which causes the reaction zone to move away from the droplet. Consequently, the temperature and concentration gradients at the droplet surface are decreased and a corresponding decrease in transfer rates results. Finally, Faeth's[8] analysis showed that the flame was particularly vulnerable to convection effects for non-adiabatic burning. Natural convection could cause larger heat losses from the flame and thus explain the abnormally high effective thermal conductivities necessary to get reasonable activation energies. These results also help to explain the data of Figure 4.1. As the ambient temperature increased, more heat was supplied to the droplet. Convection effects on the reaction zone were reduced, and the reaction zone moved closer to the droplet. This behavior was also predicted from the results of Williams[28] model, since r_c decreased with increasing ambient temperature

CHAPTER 5

SUMMARY

An experimental study of the ignition and combustion of a liquid monopropellant in an inert atmosphere was undertaken. The primary objectives of the study were:

1. To determine the effect of various ambient temperatures and pressures on the ignition delay time and burning rate of the monopropellant.

2. To propose a realistic ignition model and compare it with experimental results.

3. To check the validity of a suitable monopropellant burning theory when applied to the experimental results.

An experimental apparatus was employed which allowed testing over a range of ambient temperatures and pressures.

On the basis of preliminary tests, two heat-up models were proposed. The first model assumed the temperature of the droplet was uniform, but varying, while the second model considered temperature gradients within the droplet. Because of the approximate nature of both analyses, and their rather close agreement in predicting heat-up times, the bulk of the comparisons were made with the infinite conductivity model.

Regarding the heat-up process, it was noted that, at atmospheric pressure, ambient temperature exerts the primary influence on heat-up rates rather than preignition chemical kinetics as is the case in bipropellant ignition. At pressures of 1 atm and below, the data seemed to substantiate the boiling temperature ignition assumption. However, above 1 atm the results deviated significantly from the theoretical predictions.

Further study will be required to determine the reasons for the failure of the heat-up analysis at high pressures One possibility is that the final wet bulb temperature of the droplet may not be well represented by the boiling temperature at high pressures. While these two temperatures, roughly correspond at low pressures, this is not necessarily the case at higher pressures. Also it is possible that, at the increased heat transfer rates at higher pressures, the temperature profile near the droplet surface was very steep. Consequently, the wet bulb temperature may have been reached at the surface, while the thermocouple, located between the center and the surface, indicated a temperature significantly below the wet bulb temperature.

In the combustion study it was found that the experimental burning rates did not correlate well with Williams'[28] theory. The major assumptions of Williams'[28] theory which were violated in the test program were:

1. The activation energy was not sufficiently large to validate the thin flame assumption.
2. Natural convection may have been important in the case of non-adiabatic combustion.

It is believed that natural convection caused serious heat losses from the flame resulting in decreased mass transfer rates from the droplet.

Any future investigation of the burning rates would do well to design for adiabatic combustion. Under that condition Williams'[28] analysis could be checked solely with regard to the thin flame assumption for a range of activation energies.

Finally, it was noted that the ignition delay time was significantly longer than the burning lifetime. In particular, at high pressures the burning lifetime is so short that, after ignition (presumably at its wet bulb temperature), the droplet is consumed before its new equilibrium temperature is attained. Consequently, the entire burning process was transient in nature and the mass transfer rates were probably lower than would be expected in quasi-steady state combustion.

APPENDIX A

DERIVATION OF FINITE CONDUCTIVITY HEAT-UP MODEL

The energy equation within the droplet as given in Chapter 3 is

$$\rho C_p \frac{\partial T}{\partial t} = k \frac{1}{r^2} \frac{\partial}{\partial r}\left(r^2 \frac{\partial T}{\partial r}\right) + Q \qquad A.1$$

with the boundary conditions

$$k \frac{\partial T}{\partial r} = h (T_\infty - T), \quad r = r_E \qquad A.2$$

T is finite at $r = 0$.

Non-dimensionalize by defining

$$\theta = (T - T_o)/(T_\infty - T_o)$$

$$\eta = r/r_o$$

$$\tau = t/t_o$$

and choosing

$$t_o = \frac{\rho C_p r_o^2}{k} \quad , \quad \psi = \frac{Q r_o^2}{k(T_\infty - T_o)}$$

Eq. A.1 becomes

$$\frac{\partial \theta}{\partial \tau} = \nabla^2 \theta + \psi \qquad \text{A.3}$$

and the boundary conditions are

$$\frac{\partial \theta}{\partial \eta} = \frac{B_i}{2} (1-\theta), \quad \eta = 1 \qquad \text{A.4}$$

at $\eta = 0$, θ is finite.

Employing the Laplace transformation technique, A.3 and A.4 are transformed to the S-domain

$$\frac{d^2(\eta \bar{\theta})}{d\eta^2} - s\eta\bar{\theta} = -\frac{\eta\psi}{s} \qquad \text{A.5}$$

$$\frac{d\theta}{d\eta} = \frac{B_i}{2s} - \frac{B_i \bar{\theta}}{2} \quad , \quad \eta = 1 \qquad \text{A.6}$$

where

$$\bar{\theta} = \bar{\theta}(s, \eta) .$$

The solution of the ordinary differential Equation A.5 is

$$\eta\bar{\theta} = C_3 \sinh Z\eta + C_4 \cosh Z\eta + \frac{\eta\theta}{s^2}$$

where

$$Z = \sqrt{s} .$$

Applying the boundary condition that

$$\bar{\theta} \text{ is finite at } \eta = 0$$

then

$$C_4 = 0$$

and the equation becomes, $\eta\bar{\theta} = C_3 \sinh Z\eta + \frac{\eta\theta}{s^2}$. A.7

Differentiating Equation A.7 with respect to η

$$\frac{d\bar{\theta}}{d\eta} = C_3 \frac{(Z\eta \cosh Z\eta - \eta \sinh Z\eta)}{\eta^2} \qquad A.8$$

Now, equating A 6 and A.8 at $\eta = 1$

$$\frac{B_i}{2s} - \frac{B_i}{2}\bar{\theta} = C_3 (Z \cosh Z - \sinh Z) . \qquad A.9$$

From A.7, at $\eta = 1$

$$\bar{\theta} = C_3 \sinh Z + \frac{\psi}{s^2} . \qquad A.10$$

Substituting A.10 into A.9, and solving for C_3

$$C_3 = \frac{B_i}{2s} \frac{(1 - \psi/s)}{(Z \cosh Z + (Bi/2 - 1) \sinh Z)}$$

Substituting C_3 into A.7 we obtain the following solution for $\bar{\theta}$

$$\bar{\theta} = \frac{B_i(1 - \psi/s) \sinh Z\eta}{2\eta s(Z \cosh Z + (Bi/2 - 1) \sinh Z)} + \frac{\psi}{s^2} . \qquad A.11$$

The problem now becomes one of obtaining the inverse transform of $\bar{\theta}$.

Let $\frac{B_i}{2} - 1 = \beta$, $\frac{B_i}{2} = \alpha$.

Then

$$\bar{\theta} = \frac{\alpha \sinh Z\eta}{\eta s(Z \cosh Z + \beta \sinh Z)} - \frac{\alpha \sinh Z\eta}{\eta s^2(Z \cosh Z + \beta \sinh Z)} + \frac{1}{s^2}$$

$$= \bar{\theta}_1 - \bar{\theta}_2 + \bar{\theta}_3$$

These functions are all single-valued. Applying the inversion theorem

$$\theta(\tau,\eta) = \frac{1}{2\pi i} \lim_{\omega \to \infty} \int_{\sigma-i\omega}^{\sigma+i\omega} \bar{\theta}(s,\eta)\, e^{s\tau}\, ds$$

where the line integral is taken from A → B in the complex plane.

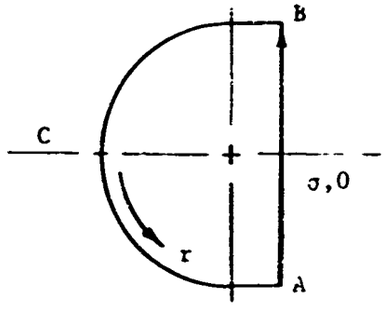

Since, as $\omega \to \infty$, the integrals over BCA disappear

$$\int_{\Gamma} \bar{\theta}(s,\eta)\, e^{s\tau} ds = \lim_{\omega \to \infty} \int_{\sigma - i\omega}^{\sigma + i\omega} \bar{\theta}(s,\eta)\, e^{s\tau} ds$$

$$= 2\pi i \sum \text{(residues within the contour)}$$

or

$$\frac{1}{2\pi i} \lim_{\omega \to \infty} \int_{\sigma - i\omega}^{\sigma + i\omega} \theta(s,\eta)\, e^{s\tau} ds = \sum \text{(residues within the contour of } \bar{\theta}\, e^{s\tau})$$

$\bar{\theta}_3$: This has a double pole at S = 0

$$\bar{\theta}_3\, e^{s\tau} = \tfrac{1}{4} e^{s\tau}/s^2$$

now for a double pole

$$R_{s_i} = \left[\frac{d}{ds} (s - s_i)^2\, \bar{\theta}\, e^{s\tau} \right]_{s} = s_i$$

thus

$$R_{\bar{\theta}_3} = \left[\frac{d}{ds} \left(\tfrac{1}{4} e^{s\tau} \right) \right]_{s=0} = \tfrac{1}{4}$$

$\bar{\theta}_1$: This has a simple pole at S = 0

$$\bar{\theta}_1 \, e^{s\tau} = \frac{\alpha \, e^{s\tau} \sinh Z\eta}{\eta s \, [Z \cosh Z + \beta \sinh Z]}$$

now for a simple pole

$$R_{s_i} = \lim_{s \to s_i} [(s-s_i) \, \theta \, e^{s\tau}]$$

thus

$$R_{\bar{\theta}_1} = \lim_{s \to 0} \left[\frac{\alpha \, e^{s\tau} \sinh Z\eta}{\eta(Z \cosh Z + \beta \sinh Z} \right] = 1 \, .$$

It has other poles, all simple, whenever

$$Z \cosh Z + \beta \sinh Z = 0$$

letting $Z = iy$

$$iy \cosh i y + \beta \sinh i y = i y \cos y + i \beta \sin y$$

or

$$\tan y = -\frac{y}{\beta} = -\frac{y}{\frac{B_1}{2} - 1}$$

Let the roots of this equation be

$$Y_N \ , \ Z_N = i\, y_N$$

now for a simple pole, if

$$\bar{\theta}\, e^{s\tau} = \frac{M(s)}{N(s)}$$

then

$$R_{s_i} = \left[\frac{M(s)}{N(s)} \right]_{s \to s_i} .$$

In our case

$$N(s) = \eta s \, [Z \cosh Z + \beta \sinh Z]$$

and the relevant part of N' is

$$\eta s \frac{d}{ds} [Z \cosh Z + \beta \sinh Z]$$

since, upon differentiating, the other part in brackets is zero at a pole.

$$\text{Now } Z = s^{\frac{1}{2}}, \quad \frac{d}{ds} = \frac{d}{dz} \frac{dz}{ds} = \frac{1}{2Z} \frac{d}{dz}$$

thus

$$N' = \frac{\eta s}{2Z} [\cosh Z + Z \sinh Z + \beta \cosh Z]$$

substituting the n^{th} root for z and collecting

$$N'_{Z=Z_N} = \frac{\eta}{2} i \, Y_N \left[\frac{B_1}{2} \cos Y_N - Y_N \sin Y_N \right] .$$

Now

$$M(s) = \alpha e^{s\tau} \sinh Z \eta$$

substituting again for z

$$M(s)_{Z=Z_N} = \alpha e^{-YN^2 \tau} i \sin Y_N \eta$$

thus

$$R_{\theta_1} = \sum_{N=1}^{\infty} \frac{2\alpha e^{-Y_N^2 \tau} \sin (Y_N \eta)}{Y_N \eta (\alpha \cos Y_N - Y_N \sin Y_N)} \quad .$$

But since $\tan Y_N = -\frac{Y_N}{\beta}$

by constructing the triangle

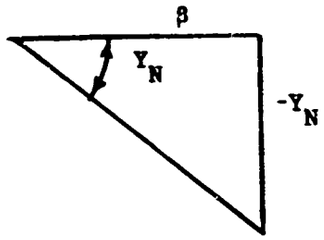

thus

$$\sin Y_N = \frac{-Y_N}{\sqrt{Y_N^2 + \beta^2}} \quad , \quad \cos Y_N = \frac{\beta}{\sqrt{Y_N^2 + \beta^2}}$$

making the appropriate substitutions

$$R_{\bar{\theta}_1} = \frac{B_i}{\eta} \sum_{N=1}^{\infty} \frac{\sqrt{Y_N^2 + \left(\frac{B_i}{2} - 1\right)^2}}{Y_N^2 + \frac{B_i}{2}\left(\frac{B_i}{2} - 1\right)} \sin\frac{(Y_N\eta)}{Y_N} e^{-Y_N^2\tau}$$

The complete transformation of $\bar{\theta}_1$ is

$$\theta_1(\tau,\eta) = 1 + \frac{B_i}{\eta} \sum_{N=1}^{\infty} \frac{\sqrt{Y_N^2 + \left(\frac{B_i}{2} - 1\right)^2}}{Y_N^2 + \frac{B_i}{2}\left(\frac{B_i}{2} - 1\right)} \frac{\sin(Y_N\eta)}{Y_N} e^{-Y_N^2\tau}$$

$\bar{\theta}_2$: Now

$$\bar{\theta}_2 = \frac{\Psi}{s} \bar{\theta}_1$$

and

$$L^{-1} \frac{1}{s} F(s) = \int_0^{\tau} F(x)\, dx$$

thus

$$\theta_2(\tau,\eta) = \psi\left[\tau + \frac{B_i}{\eta} \sum_{N=1}^{\infty}\left(\frac{\sqrt{Y_N^2+\left(\frac{B_i}{2}-1\right)^2}}{Y_N^2+\frac{B_i}{2}\left(\frac{B_i}{2}-1\right)} \frac{\sin(Y_N\eta)}{Y_N}\right)\left(\frac{1-e^{-Y_N^2\tau}}{Y_N^2}\right)\right]$$

adding the partial solutions

$$\theta_{(\tau,\eta)} = \theta_1(\tau,\eta) - \theta_2(\tau,\eta) + \theta_3(\tau,\eta)$$

The complete solution is

$$\theta_{(\tau,\eta)} = 1 - \frac{B_i}{\eta} \sum_{N=1}^{\infty} \frac{\sqrt{Y_N+\left(\frac{B_i}{2}-1\right)^2}}{Y_N^2+\frac{B_i}{2}\left(\frac{B_i}{2}-1\right)} \frac{\sin(Y_N\eta)}{Y_N^3}\left[Y_N^2 e^{-Y_N^2\tau} - \psi\left(1-e^{-Y_N^2\tau}\right)\right]$$

APPENDIX B

FLUID AND GAS PROPERTIES

B1 Fluid Properties

Property	Value	Source or Method of Calculation
Density	86 LBM/FT^3 at 20°C	de C. Crater[6], Beilstein[4]
Specific Heat	4.14 BTU/LBMR at 20°C	Calc.-Johnson and Huang[21] Method
Latent Heat of Vaporization	158 BTU/LBM	Calc. Giacalone[21] Method
Critical Pressure	35.8 ATM	Calc. Lydersen[21] Method
Critical Temperature	1070°R	From Vapor Pressure Curve at Critical Pressure
Thermal Conductivity	9.50×10^2 $\frac{BTU}{FT\ HR\ ^\circ R}$ @ 20°C	Calc. Weber[21] Method
Heat of Combustion	-2000 BTU/LBM	From Oxygen Balance Curve[2]

B2 Gas Properties

Specific Heat	~.56 $\frac{BTU}{LBM^{\circ}R}$ at $2500^{\circ}R$	Cal. Bennewitz and Rossner[21] Method
Heat-Up Thermal Conductivity	Assume $k_{n_2} = k_{air}$	Keenan and Kay[11]
Burning Thermal Conductivity	.054 $\frac{BTU}{FT\ HR^{\circ}R}$ at $2500^{\circ}R$	Johnson-Huang[10] Chart using Viscosity Cal. by Bromley-Wilke[21] Method

BIBLIOGRAPHY

1. Adams, G. K., and Bawn, C. E. H., "The Homogeneous Decomposition of Ethyl Nitrate", Transactions of the Faraday Society, Vol. 45, pp. 494-499 (1949).

2. Altman, D., Carter, J. M., Penner, S. S., and Summerfield, M., Liquid Propellant Rockets (Princeton University Press, Princeton, N. J., 1960), pp 82-97.

3. Barrere, M. and Moutet, H., "Etude Experimentale de la Combustion de Gouttes de Monergol", La Recherche Aeronautique, Vol. 50, pp. 31-38 (March-April 1956).

4. Beilstein's Handbuch Der Organischen Chemie 4 Auflang Band 1, Sweiter Teil (Springer-Verlag, Berlin, 1958), pp 2149

5. Benson, S. W., The Foundations of Chemical Kinetics, (McGraw Hill Book Company, Inc., New York, 1960), pp 419-424.

6. Crater, W. deC., "The Vapor Pressure of Glycerol Trinitrate and Certain Glycol Dinitrates", Industrial and Engineering Chemistry, Vol. 21, No. 7, pp 674-676 (1929).

7. Faeth, G. M., The Kinetics of Droplet Ignition in a Quiescent Air Environment, (The Pennsylvania State University, Ph.d. Thesis, Dept. of Mechanical Engineering, 1964).

8. Faeth, G. M., "Monopropellant Droplet Burning at Low Reynolds Numbers", to be published in Combustion and Flame.

9. Hottel, H. C., Williams, G. C., and Simpson, H C., "Combustion of Drops of Heavy Liquid Fuels", 5th Symposium on Combustion, (Reinhold, New York, 1955) pp 101-124 .

10. Johnson, A. I., and Huang, C J., "Thermal Conductivity Chart for Gases", Chemical Engineering, Vol 61 , pp 204-205 (1954).

11. Keenan, J H., and Kay, J., Gas Tables, (John Wiley and Sons, Inc., New York, 1963) pp 34.

12. Kobayasi, K., "An Experimental Study on the Combustion of a Fuel Droplet", 5th Symposium on Combustion, (Reinhold, New York, 1955) pp 141-148.

13. Kreith, F., Principles of Heat Transfer, (International Textbook Company, Scranton, Pa., 1958) p 536.

14. Lange, N. A., ed., Handbook of Chemistry, (Handbook Publishers, Inc., Sandusky, Ohio, 1952), 8th Edition, pp 1463-1484.

15. Levy, J. B., "The Thermal Decomposition of Nitrate Esters, 1 Ethyl Nitrate', Journal of the American Chemical Society, Vol. 76, pp 3254-3257 (1954).

16. Lorell, J., and Wise, H., "Steady State Burning of a Liquid Droplet. 1. Monopropellant Flame" Journal of Chemical Physics, Vol. 23, No. 10, pp 1928-1932, (1955).

17. Nishiwaki, N., "Kinetics of Liquid Combustion Processes: Evaporation and Ignition Lag of Fuel Droplets", 5th Symposium on Combustion, (Reinhold, New York, 1955) pp 148-158.

18. Phillips, L., "Thermal Decomposition of Organic Nitrates", Nature Vol. 160, pp 753-754, (1947).

19. Phillips, L., "Thermal Decomposition of Organic Nitrates', Nature Vol. 654 (1950).

20. Ranz, W. E. and Marshall, W. R., Jr., "Evaporation from Drops', Chem. Eng. Prog., Vol. 48, pp 141-146, 173-180 (1952).

21. Reid, R. C. and Sherwood, T. K., The Properties of Gases and Liquids, (McGraw-Hill Book Company, Inc., New York, 1958) pp 72, 140-143, 222-228.

22. Rosser, W. A., 'The Decomposition Burning of Monopropellant Drops: Hydrazine, Nitromethane, and Ethyl Nitrate", Prog. Rept. 20-305, California Institute of Technology, J. P. L., Pasadena (1957).

23. Schneider, P. J., Conduction Heat Transfer, (Addison-Wesley Publishing Company, Inc., Reading, Mass., 1955).

24. Spalding, D. B. and Jain, V. K., "Theory of the Burning of Monopropellant Droplets', A.R.C Technical Report, Current Paper No. 447, (1959).

25. Spalding, D. B., "The Theory of Steady Laminar Spherical Flame Propagation: Equations and Numerical Solution", Combustion and Flame, Vol. 4, pp 51-58 (1960).

26. Tarifa, C. S., del Notario, P. P., and Moreno, F. G., "Combustion of Liquid Monopropellants and Bipropellants in Droplets", 8th International Symposium on Combustion, (Williams and Wilkins Co., Baltimore, 1962) pp 1035-1056.

27. Williams, F. A., 'On the Assumptions Underlying Droplet Vaporization and Combustion Theories', The Journal of Chemical Physics, Vol. 33, No. 1, pp 133-144 (July 1960)

28. Williams, F. A., Combustion Theory, (Addison-Wesley Publishing Company, Inc., New York, 1958) pp 231-249.